Research Article | Vol. 9, No. 4 | 1 Apr 2018 | BIOMEDICAL OPTICS EXPRESS 1531
Biomedical Optics EXPRESS

Modelling spatially-resolved diffuse reflectance spectra of a multi-layered skin model by artificial neural networks trained with Monte Carlo simulations

SHENG-YANG TSUI,[1] CHIAO-YI WANG,[2] TSAN-HSUEH HUANG,[2] AND KUNG-BIN SUNG[1,2,*]

[1]*Department of Electrical Engineering, National Taiwan University, Taipei, Taiwan*
[2]*Graduate Institute of Biomedical Electronics and Bioinformatics, National Taiwan University, Taipei, Taiwan*
[*]*kbsung@ntu.edu.tw*

Abstract: A robust modelling method was proposed to extract chromophore information in multi-layered skin tissue with spatially-resolved diffuse reflectance spectroscopy. Artificial neural network models trained with a pre-simulated database were first built to map geometric and optical parameters into diffuse reflectance spectra. Nine fitting parameters including chromophore concentrations and oxygen saturation were then determined by solving the inverse problem of fitting spectral measurements from three different parts of the skin. Compared to the Monte Carlo simulation accelerated by a graphics processing unit, the proposed modelling method not only reduced the computation time, but also achieved a better fitting performance.

OCIS codes: (170.3660) Light propagation in tissues; (170.6510) Spectroscopy, tissue diagnostics; (200.4260) Neural networks.

References and links

1. I. J. Bigio and J. R. Mourant, "Ultraviolet and visible spectroscopies for tissue diagnostics: fluorescence spectroscopy and elastic-scattering spectroscopy," Phys. Med. Biol. **42**(5), 803–814 (1997).
2. U. Utzinger and R. R. Richards-Kortum,"Fiber optic probes for biomedical optical spectroscopy," J. Biomed. Opt. **8**(1), 121–147 (2003).
3. I. J. Bigio and S. G. Bown, "Spectroscopic sensing of cancer and cancer therapy: current status of translational research," Cancer Biol. Ther. **3**(3), 259–267 (2004).
4. G. Zonios, A. Dimou, I. Bassukas, D. Galaris, A. Tsolakidis, and E. Kaxiras, "Melanin absorption spectroscopy: new method for noninvasive skin investigation and melanoma detection," J. Biomed. Opt. **13**(1), 014017 (2008).
5. V. V. Tuchin, *Tissue Optics*: *Light Scattering Methods and Instruments for Medical Diagnosis* (SPIE, 2015).
6. R. A. J. Groenhuis, H. A. Ferwerda, and J. J. Ten Bosch, "Scattering and absorption of turbid materials determined from reflection measurements. 1: theory," Appl. Opt. **22**(16), 2456–2462 (1983).
7. L. Wang, S. L. Jacques, and L. Zheng, "MCML–Monte Carlo modeling of light transport in multi-layered tissues," Comput. Methods Programs Biomed. **47**(2), 131–146 (1995).
8. C. Zhu and Q. Liu, "Review of Monte Carlo modeling of light transport in tissues," J. Biomed. Opt. **18**(5), 50902 (2013).
9. D. Yudovsky and L. Pilon, "Simple and accurate expressions for diffuse reflectance of semi-infinite and two-layer absorbing and scattering media," Appl. Opt. **48**(35), 6670–6683 (2009).
10. D. Yudovsky and L. Pilon, "Rapid and accurate estimation of blood saturation, melanin content, and epidermis thickness from spectral diffuse reflectance," Appl. Opt. **49**(10), 1707–1719 (2010).
11. I. Fredriksson, M Larsson, and T. Strömberg, "Inverse Monte Carlo method in a multilayered tissue model for diffuse reflectance spectroscopy," J. Biomed. Opt. **17**(4), 047004 (2012).
12. X. Zhong, X. Wen, and D. Zhu,"Lookup-table-based inverse model for human skin reflectance spectroscopy: two-layered Monte Carlo simulations and experiments," Opt. Express **22**(2), 1852–1864 (2014).
13. M. Sharma, R. Hennessy, M. K. Markey, and J. W. Tunnell, "Verification of a two-layer inverse Monte Carlo absorption model using multiple source-detector separation diffuse reflectance spectroscopy," Biomed. Opt. Express **5**(1), 40–53 (2014).
14. Q. Wang, D. Le, J. Ramella-Roman, and J. Pfefer, "Broadband ultraviolet-visible optical property measurement in layered turbid media," Biomed. Opt. Express **3**(6), 1226–1240 (2012).

#319276 https://doi.org/10.1364/BOE.9.001531
Journal © 2018 Received 8 Jan 2018; revised 21 Feb 2018; accepted 1 Mar 2018; published 7 Mar 2018

Biomedical Optics EXPRESS

15. D. Yudovsky and A. J. Durkin, "Spatial frequency domain spectroscopy of two layer media," J. Biomed. Opt. **16**(10), 107005 (2011).
16. D. Yudovsky, J. Q. Nguyen, and A. J. Durkin, "*In vivo* spatial frequency domain spectroscopy of two layer media," J. Biomed. Opt. **17**(10), 107006 (2012).
17. Y. H. Liao, S. Y. Chen, S. Y. Chou, P. H. Wang, M. R. Tsai, and C. K. Sun, "Determination of chronological aging parameters in epidermal keratinocytes by *in vivo* harmonic generation microscopy," Biomed. Opt. Express **4**(1), 77–88 (2013).
18. Y. H. Hsiao, G. H. Tien, M. J. Chuang, F. W. Hsu, H. P. Hsieh, and K. B. Sung, "Development of a movable diffuse reflectance spectroscopy system for clinical study of esophageal precancer," Proc. SPIE **9537**, 95371Q (2015).
19. A. N. Bashkatov, E. A. Genina, and V. V. Tuchin, "Optical properties of skin, subcutaneous, and muscle tissues: a review," J. Innov. Opt. Health Sci. **4**(1), 9–38 (2011).
20. S. L. Jacques, "Optical properties of biological tissues: a review," Phys. Med. Biol. **58**(11), R37–R61 (2013).
21. K Chopra, D. Calva, M. Sosin, K. K. Tadisina, A. Banda, C. De La Cruz, M. R. Chaudhry, T. Legesse, C. B. Drachenberg, P. N. Manson, and M. R. Christy, "A comprehensive examination of topographic thickness of skin in the human face," Aesthet. Surg. J. **35**(8), 1007–1013 (2015).
22. L. Wang and S. L. Jacques, *Monte Carlo Modeling of Light Transport in Multi-Layered Tissues in Standard C* (Anderson Cancer Center, University of Texas M. P. Anderson Cancer Center, Houston, Texas, 1992).
23. E. Alerstam, T. Svensson, and S. Andersson-Engels, "Parallel computing with graphics processing units for high-speed Monte Carlo simulation of photon migration," J. Biomed. Opt. **13**(6), 060504 (2008).
24. J. W. Su, W. C. Hsu, J. W. Tjiu, C. P. Chiang, C. W. Huang, and K. B. Sung, "Investigation of influences of the paraformaldehyde fixation and paraffin embedding removal process on refractive indices and scattering properties of epithelial cells," J. Biomed. Opt. **19**(7), 75007 (2014).
25. I. V. Meglinski and S. J. Matcher, "Quantitative assessment of skin layers absorption and skin reflectance spectra simulation in the visible and near-infrared spectral regions," Physiol. Meas. **23**(4), 741–753 (2002).
26. J. Qu, C. Macaulay, S. Lam, and B. Palcic, "Optical properties of normal and carcinomatous bronchial tissue," Appl. Opt. **33**(31), 7397–7405 (1994).
27. S. L. Jacques and D. J. McAuliffe, "The melanosome: threshold temperature for explosive vaporization and internal absorption coefficient during pulsed laser irradiation," Photochem. Photobiol. **53**(6), 769–775 (1991).
28. A. S. Nunez, "A physical model of human skin and its application for search and rescue," (DTIC Document, 2009).
29. H. Buiteveld, J. H. M. Hakvoort, and M. Donze, "The optical properties of pure water," Proc. SPIE **2258**, 174–183 (1994).
30. S. Prahl, "Optical absorption of hemoglobin," http://omlc.ogi.edu/spectra/hemoglobin/hemestruct/index.html.
31. S. L. Jacques, "Origins of tissue optical properties in the UVA, visible, and NIR regions," OSA TOPS on *Advances in Optical Imaging and Photon Migration*, Vol. 2, R. R. Alfano and James G. Fujimoto, eds. (Optical Society of America, 1996), pp. 364-371.
32. K. B. Sung and H. H. Chen, "Enhancing the sensitivity to scattering coefficient of the epithelium in a two-layered tissue model by oblique optical fibers: Monte Carlo study," J. Biomed. Opt. **17**(10), 107003 (2012).
33. K. B. Sung, K. W. Shih, F. W. Hsu, H. P. Hsieh, M. J. Chuang, Y. H. Hsiao, Y. H. Su, and G. H. Tien, "Accurate extraction of optical properties and top layer thickness of two-layered mucosal tissue phantoms from spatially resolved reflectance spectra," J. Biomed. Opt. **19**(7), 077002 (2014).
34. T. Y. Tseng, C. Y. Chen, Y. S. Li, and K. B. Sung, "Quantification of the optical properties of two-layered turbid media by simultaneously analyzing the spectral and spatial information of steady-state diffuse reflectance spectroscopy," Biomed. Opt. Express **2**(4), 901–914 (2011).
35. N. Rajaram, T. H. Nguyen, and J. W. Tunnell, "Lookup table-based inverse model for determining optical properties of turbid media," J. Biomed. Opt. **13**(5), 050501 (2008).
36. R. Hennessy, S. L. Lim, M. K. Markey, and J. W. Tunnell, "Monte Carlo lookup table-based inverse model for extracting optical properties from tissue-simulating phantoms using diffuse reflectance spectroscopy," J. Biomed. Opt. **18**(3), 037003 (2013).
37. A. Kienle, L. Lilge, M. S. Patterson, R. Hibst, R. Steiner, and B. C. Wilson, "Spatially resolved absolute diffuse reflectance measurements for noninvasive determination of the optical scattering and absorption coefficients of biological tissue," Appl. Opt. **35**(13), 2304–2314 (1996).
38. T. J. Pfefer, L. S. Matchette, C. L. Bennett, J. A. Gall, J. N. Wilke, A. J. Durkin, and M. N. Ediger, "Reflectance-based determination of optical properties in highly attenuating tissue," J. Biomed. Opt. **8**(2), 206–215 (2003).
39. D. Sharma, A. Agrawal, L. S. Matchette, and T. J. Pfefer, "Evaluation of a fiberoptic-based system for measurement of optical properties in highly attenuating turbid media," Biomed. Eng. Online **5**, 49 (2006).
40. D. Warncke, E. Lewis, S. Lochmann, and M. Leahy, "A neural network based approach for determination of optical scattering and absorption coefficients of biological tissue," J. Phys.: Conf. Ser. **178**, 012047 (2009).
41. L. Zhang, Z. Wang, and M. Zhou, "Determination of the optical coefficients of biological tissue by neural network," J. Mod. Opt. **57**(13), 1163–1170 (2010).
42. Q. Wang, K. Shastri, and T. J. Pfefer, "Experimental and theoretical evaluation of a fiber-optic approach for optical property measurement in layered epithelial tissue," Appl. Opt. **49**(28), 5309–5320 (2010).
43. Y. W. Chen and S. H. Tseng, "Efficient construction of robust artificial neural networks for accurate determination of superficial sample optical properties," Biomed. Opt. Express **6**(3), 747–760 (2015).

Biomedical Optics EXPRESS

44. R. Reif, O. A'Amar, and I. J. Bigio, "Analytical model of light reflectance for extraction of the optical properties in small volumes of turbid media," Appl. Opt. **46**(29), 7317–7328 (2007).
45. G. Zonios and A. Dimou, "Modeling diffuse reflectance from homogeneous semi-infinite turbid media for biological tissue applications: a Monte Carlo study," Biomed. Opt. Express **2**(12), 3284–3294 (2011).
46. G. Mantis and G. Zonios, "Simple two-layer reflectance model for biological tissue applications," Appl. Opt. **48**(18), 3490–3496 (2009).
47. G. Zonios and A. Dimou, "Simple two-layer reflectance model for biological tissue applications: lower absorbing layer," Appl. Opt. **49**(27), 5026–5031 (2010).
48. Y. W. Chen, C. C. Chen, P. J. Huang, and S. H. Tseng, "Artificial neural networks for retrieving absorption and reduced scattering spectra from frequency-domain diffuse reflectance spectroscopy at short source-detector separation," Biomed. Opt. Express **7**(4), 1496–1510 (2016).
49. D. J. Cuccia, F. Bevilacqua, A. J. Durkin, F. R. Ayers, and B. J. Tromberg, "Quantitation and mapping of tissue optical properties using modulated imaging," J. Biomed. Opt. **14**(2), 024012 (2009).
50. N. Bedard, R. A. Schwarz, A. Hu, V. Bhattar, J. Howe, M. D. Williams, A. M. Gillenwater, R. Richards-Kortum, and T. S. Tkaczyk, "Multimodal snapshot spectral imaging for oral cancer diagnostics: a pilot study," Biomed. Opt. Express **4**(6), 938–949 (2013).

1. Introduction

Diffuse reflectance spectroscopy (DRS) is widely used to measure optical properties of tissue such as absorption and scattering coefficients. It is successfully applied for noninvasively characterization of biological tissue, morphological investigation, and diagnosis of diseases [1–5]. To extract optical properties from spectral measurements, an accurate model is required to resolve forward and inverse relationship between a set of optical properties and its corresponding diffuse reflectance spectra. The diffuse approximation was first introduced to analytically model the diffuse reflectance emitted from tissue [6]. However, the diffuse theory suffers from many limitations such as assumptions on high scattering medium and sufficiently large separations between the light source and the detector. Monte Carlo (MC) simulations have been developed and used as a gold standard approach to overcome the shortcomings of the diffuse theory [7]. Since the MC simulation relies on repeated random sampling to describe the radiative transfer process, it inevitably requires sufficient computation time to obtain accurate results. Some researchers have proposed many methods to accelerate simulations [8], but it is still time-consuming to inversely determine tissue optical properties, especially for superficial multi-layered tissue models.

Therefore, several methods based on pre-simulated MC databases have been proposed to obtain the diffuse reflectance and optical properties efficiently including semi-empirical/empirical models (SE/EMs), look-up table (LUT), inverse artificial neural network (I-ANN) and forward artificial neural network (F-ANN). For example, Yudovsky and Pilon provided a general semi-empirical model for two-layered semi-infinite tissue based on two flux approximations [9, 10]. Parameters appearing in the analytic expressions were fitted to match results from MC simulations. The model would then be used to inversely resolve chromophore information for two-layered skin tissue. Fredriksson *et al.* proposed an efficient method of modelling the diffuse reflectance spectrum for three-layered skin tissue by linearly interpolating path length distributions from 72 base simulations [11]. Beer-Lambert's law was applied to calculate absorptions for each path length, and a total of nine fitting parameters were utilized to solve the inverse problem. Zhong *et al.* and Sharma *et al.* developed a look-up table based on two-layered MC simulations to inversely evaluate physiological characteristics of skin tissue [12, 13]. The numerical model could efficiently and accurately determine volume fraction of melanin, volume fraction of blood, and oxygen saturation from spectral measurements. Wang *et al.* constructed I-ANN models trained with condensed MC simulations to directly obtain optical coefficients for a two-layered superficial tissue model [14]. F-ANN models were introduced by Yudovsky and Durkin to map a set of geometric properties and optical coefficients into spatial frequency domain diffuse reflectance [15, 16]. Iterative curve-fitting method was then applied to find an optimal set of chromophore concentrations and oxygen saturation for a superficial two-layered skin model.

Biomedical Optics EXPRESS

The objective of this study is to present an efficient method capable of estimating scattering coefficients and chromophore information in multi-layered skin tissue from spatially-resolved diffuse reflectance spectra. First, F-ANN models trained with a pre-simulated database were built to map nine input parameters including three thicknesses and six optical coefficients into spatially-resolved diffuse reflectance spectra. Thicknesses of the stratum corneum and two other epidermal layers were measured by *in vivo* harmonic generation microscopy (HGM) [17], and *in vivo* diffuse reflectance spectra were obtained with a custom-built DRS system [18]. Nine fitting parameters appearing in wavelength-dependent expressions were then determined by solving the inverse problem of fitting spectral measurements. A flowchart of our proposed method is shown in Fig. 1.

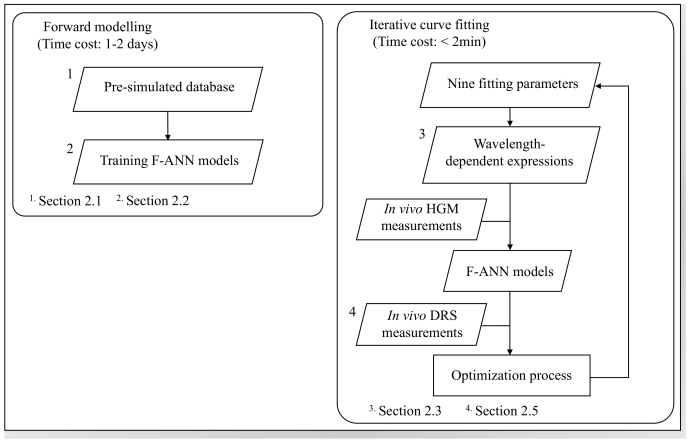

Fig. 1. The flowchart of the forward modelling and the iterative curve fitting to solve the inverse problem.

2. Methods, models and measurements

2.1. Pre-simulated database

Multi-layered skin tissue was assumed to contain four homogenous layers (i.e., stratum corneum, intermediate epidermis without melanin, basal epidermis with melanin, and dermis). The stratum corneum was a keratinized superficial layer, and the intermediate epidermal layer consisted of the stratum granulosum and the stratum spinosum. A high concentration of melanin was located within the basal epidermal layer [17]. The geometric and optical parameters over visible wavelengths were considered to cover a wide range for the skin tissue model as summarized in Table 1 [19–21]. The thicknesses of the upper three layers varied from 5 to 30, 5 to 30, 10 to 60 μm respectively, and the thickness of the dermis was assumed to be infinite. The scattering coefficients of the lower two epidermal layers (μ_{s2}, μ_{s3}) were set to have a fixed ratio, and the absorption coefficients of the upper two layers (μ_{a1}, μ_{a2}) were assumed to be the same. Anisotropy factors of the Henyey-Greenstein scattering phase function (g_x) were selected to be 0.92, 0.75, 0.75 and 0.715 from upper to lower layers. All layers had an equal refractive index of 1.42.

Simulations of light transport in the multi-layered skin model were performed using public MCML code [22] with modifications to accelerate the computation by the graphics processing unit (GPU, GeForce GTX 1080) [23]. A Gaussian beam consisting of 100 million photons was used as the incident light perpendicular to the tissue surface. The diffuse reflectance remitted from the tissue surface was collected by three optical fibers which were separated from the source fiber by distances (SDS) of 0.22 mm, 0.45 mm and 0.73 mm, respectively. All fibers had a core diameter of

Biomedical Optics EXPRESS

0.2 mm and a core refractive index of 1.457 with a numerical aperture of 0.26, and were in gentle contact with skin tissue. The nine input parameters ($th_1, th_2, th_3, \mu_{a1}, \mu_{s1}, \mu_{s2}, \mu_{a3}, \mu_{a4}, \mu_{s4}$) were randomly assigned within the setting range for each MC simulation, and a total of 30,000 samples were then created as a pre-simulated database.

Table 1. Setting ranges of input geometric and optical parameters.

	$th_x(\mu m)$	$\mu_{ax}(cm)^{-1}$	$\mu_{sx}(cm)^{-1}$	g_x
Stratum corneum (x=1)	5-30	0.1-5	100-1000	=0.920
Intermediate epidermal layer (x=2)	5-30	$=\mu_{a1}$	10-500	=0.750
Basal epidermal layer (x=3)	10-60	1-350	$=1.35\mu_{s2}$	=0.750
Dermis (x=4)	=Inf	0.01-15	10-500	=0.715

2.2. Forward ANN model

Three F-ANN models, one for each SDS, were built using the Neural Network Toolbox (The MathWorks, Inc.). The models consisted of an input layer, double hidden layers with neurons varied from 15 to 85 and an output layer. The nine input parameters from the pre-simulated database were first normalized by linearly mapping minimum and maximum values to [-1 1]. The weights and biases in the model were tuned by minimizing the relative error between the estimated and the target reflectance. The log-sigmoid function was chosen as the transfer function to generate outputs for the subsequent layers including the final output layer. The scaled conjugate gradient algorithm was used to train the F-ANN models. During the training process, the database was randomly divided into three subsets (i.e., 70% for the training set, 15% for the validation set, and 15% for the testing set). The training set was used to optimize the models and estimate diffuse reflectance, the validation set was monitored to avoid overfitting, and the testing set was used to evaluate the performance of the trained models.

2.3. Wavelength-dependent expressions for optical coefficients

2.3.1. Stratum corneum, intermediate and basal epidermal layers

The scattering coefficients of the upper two layers (μ_{s1}, μ_{s2}) were both assumed to have a power law relation with the wavelength as commonly done for biological tissues [20]:

$$\mu_{sx} = \frac{C_x \lambda^{-b_x}}{1 - g_x} (x = 1, 2), \tag{1}$$

where C_x and b_x are fitting parameters; λ is the wavelength in nm; g_x is the anisotropy factor. Our previous study found a high scattering coefficient in the uppermost keratin layer of oral epithelial tissue using quantitative phase images of thin tissue slices. In addition, the scattering coefficients of the basal and intermediate layers approximately had a fixed ratio of 1.35 [24]. Since the depth-dependent morphology of epithelial cells in the oral epithelium is similar to that of epidermal cells in the skin and the scattering coefficient is highly correlated with the morphology, we assumed that the scattering coefficients of the basal and intermediate epidermal layers (μ_{s2}, μ_{s3}) also had the same ratio.

The absorptions of the upper two layers (μ_{a1}, μ_{a2}) were assumed to be approximately the same as epithelial cells because these layers had negligible melanin [17, 25]; as a result, the absorption coefficients could be expressed as:

$$\mu_{a1} = \mu_{a2} = \mu_{a,e}(\lambda), \tag{2}$$

where $\mu_{a,e}(\lambda)$ is the absorption coefficient measured from thin slices of bronchus epithelial tissue [26].

Biomedical Optics EXPRESS

Melanin has a broad absorption spectrum exhibiting stronger absorption at shorter wavelengths. This dominant absorber was assumed to exist only in the basal layer of the epidermis whose absorption coefficient (μ_{a3}) could be calculated as:

$$\mu_{a3} = f_m \mu_{a,m}(\lambda) + (1 - f_m)\mu_{a,e}(\lambda), \tag{3}$$

where f_m is the volume fraction of melanin and $\mu_{a,m}(\lambda)$ is the absorption coefficient of melanin given by [27]:

$$\mu_{a,m}(\lambda) = 1.7 \times 10^{12} \lambda^{-3.48} (cm^{-1}) \tag{4}$$

2.3.2. Dermis

The scattering coefficient of the dermis (μ_{s4}) was also expressed as:

$$\mu_{s4} = \frac{C_3 \lambda^{-b_3}}{1 - g_4}, \tag{5}$$

where C_3 and b_3 are fitting parameters.

The absorption coefficient of the dermis (μ_{a4}) was modeled as a combination of the absorption of blood, water and collagen [28]:

$$\mu_{a4} = f_b \mu_{a,b}(\lambda) + f_w \mu_{a,w}(\lambda) + (1 - f_b - f_w)\mu_{a,c}(\lambda), \tag{6}$$

where f_b is the average volume fraction of blood; f_w is the volume fraction of water which was assumed to have a fixed value of 70% [19]; $\mu_{a,b}(\lambda), \mu_{a,w}(\lambda), \mu_{a,c}(\lambda)$ are the absorption coefficients of blood, water and collagen, respectively. The absorption coefficients measured from pure water and gelatin sheets with 100% collagenous protein were used for $\mu_{a,w}(\lambda)$ and $\mu_{a,c}(\lambda)$, respectively [28, 29]. $\mu_{a,b}(\lambda)$ is formed by summing the absorption coefficients of oxy-hemoglobin ($\mu_{a,oxy}$) and deoxy- hemoglobin ($\mu_{a,deoxy}$), which are given by [30]:

$$\mu_{a,oxy}(\lambda) = 2.303 \varepsilon_{oxy}(\lambda) C_{heme} S / 64,532 \; and \tag{7}$$

$$\mu_{a,deoxy}(\lambda) = 2.303 \varepsilon_{deoxy}(\lambda) C_{heme} (1 - S) / 64,500, \tag{8}$$

where $\varepsilon_{oxy}(\lambda)$ and $\varepsilon_{deoxy}(\lambda)$ are known molar extinction coefficients of oxy-hemoglobin and deoxy-hemoglobin, respectively; C_{heme} represents the hemoglobin concentration of blood which is typically assumed to be 150 g/l; S (%) is the unknown oxygen saturation [30].

2.4. Iterative curve-fitting method

According to the review of the literature [19, 28, 31], the values of nine fitting parameters ($C_1, b_1, C_2, b_2, C_3, b_3, f_m, f_b, S$) were constrained between the upper and lower bounds as shown in Table 2. The setting ranges of μ_{a3} and μ_{a4} in Table 1 were chosen to cover the values of the absorption coefficients generated by the bounded parameters (f_m, f_b, S) while the fitting parameters for scattering coefficients ($C_1, b_1, C_2, b_2, C_3, b_3$) were non-linearly constrained to ensure that the scattering coefficients would fall within the setting range of μ_{s1}, μ_{s2} and μ_{s4}. An initial guess of the fitting parameters was randomly assigned to generate optical coefficients based on Eqs. (1)-(8). The optical coefficients combined with the thicknesses obtained from HGM images were fed into the trained F-ANN models to estimate diffuse reflectance spectra. The Matlab built-in function "fmincon" then optimized the fitting parameters by minimizing an objective function which was defined as the root-mean-squared percent error between the estimated and the measured diffuse reflectance spectra:

Biomedical Optics EXPRESS

$$RMSE = \sqrt{\frac{\sum_{j=1}^{l}\sum_{i=1}^{k}[(\frac{R_{i,j}-r_{i,j}}{r_{i,j}})\times 100]^2}{l\times k}}\%, \quad (9)$$

where l and k were the total number of fibers and wavelengths analyzed, respectively; R and r represented the estimated and the measured diffuse reflectance spectra. The fitting function stopped the optimization process when the current step size was less than a step tolerance of 10^{-7}. The above random guess and fitting process were repeated for 100 times to find an optimal local minimum.

Table 2. Lower and upper bounds for fitting parameters.

	$C_1(\text{cm})^{-1}$	b_1	$C_2(\text{cm})^{-1}$	b_2	$C_3(\text{cm})^{-1}$	b_3	f_m	f_b	S
Lower bound	1×10^5	1	1×10^5	1	1×10^5	1	1%	0.0%	0.0%
Upper bound	5×10^6	2	5×10^6	2	5×10^6	2	25%	0.5%	100%

2.5. Spatially-resolved diffuse reflectance spectra of skin tissue

The diffuse reflectance spectra were acquired by a custom-built DRS system which shined white light (410-760 nm). The setup of the source and detectors was the same as those described in Sec. 2.1. We used a set of five homogeneous aqueous phantoms to calibrate the diffuse reflectance spectra and to establish calibration factors for removing the effects of non-uniform spectral response and background of the system. The tissue mimicking phantoms were made of known concentrations of polystyrene beads (Polysciences, Inc., Polybead Microspheres) and hemoglobin (Sigma-Aldrich, ferrous stabilized human hemoglobin). The calibration phantoms contained polystyrene beads with a diameter of 0.51±0.008 μm at concentrations of 9.10×10^{10}, 5.60×10^{10}, 3.64×10^{10}, 2.28×10^{10}, and 1.21×10^{10} particles/ml, respectively. The first four phantoms and the last phantom also contained hemoglobin at concentrations of 0.056 and 0.1126 mg/ml respectively. Scattering coefficients and absorption coefficients of the phantoms were obtained using Mie theory and UV-visible absorption spectroscopy measurements, respectively. With the known optical coefficients, a linear calibration relation was then established by comparing the measured diffuse reflectance of the phantoms to the simulated diffuse reflectance. In this study, experiments using the DRS and the HGM system were approved by the Institutional Review Board at National Taiwan University Hospital, and the informed consent was obtained from healthy volunteers.

3. Results

3.1. The training results of F-ANN models

The critical point of this study was to build F-ANN models that accurately mapped geometric and optical parameters into diffuse reflectance at several SDSs. There were two factors that greatly influenced the accuracy of F-ANN models: (1) the sample size used in the training process and (2) the coefficient of variation (CV) of MC simulations. We had used several sample sizes from 3,500 to 21,000 to train F-ANN models with 55 neurons for each hidden layer. The absolute relative error between the estimated and the target reflectance gradually converged to a minimum, and a total of 21,000 samples were enough to build robust F-ANN models without sacrificing the performance. The accuracy of F-ANN models for each SDS with various hidden neurons was summarized in Table 3. The errors of the best models were 1.28%±1.19%, 2.27%±2.40% and 3.59%±4.27% for the SDS of 0.22 mm, 0.45 mm and 0.73 mm, respectively. The curves of training, validation and testing error for each training epoch were depicted in Fig. 2(a).

Biomedical Optics EXPRESS

In addition, the CV of MC simulations would induce the uncertainty in the F-ANN models to predict the diffuse reflectance. The value of CV at a specific reflectance value was estimated by conducting a random process for 20 times. The random process repeated 10^8 times an event of which the occurrence probability was equal to the probability of a photon collected by the fiber. The curve of CV versus reflectance was then obtained and plotted in Fig. 2(b). Furthermore, we used the F-ANN models with minimal errors to generate the diffuse reflectance for each sample in the training and the testing set. The curves of error versus reflectance in Fig. 2(b) were acquired by averaging the absolute relative errors of the samples in each reflectance bin of the histograms as shown in Figs. 2(c) and 2(d). The curves demonstrated that the error had a negative correlation with the value of the diffuse reflectance, and was highly correlated with the CV of MC simulations. According to Fig. 2(b), the error in the testing set reached around 30% at the reflectance of 10^{-8} which occurred in highly absorbing media (i.e., μ_{a3}>300 and μ_{a4}>10). To solve this issue, 1177 samples in the database with the reflectance lower than 10^{-7} at the SDS of 0.73 mm were re-simulated by launching one billion photons to reduce the variation in simulated diffuse reflectance. F-ANN models for the SDS of 0.73 mm were then re-trained and re-tested with the updated database. The results, as summarized in Table 3, showed that the mean and the standard deviation of the absolute relative errors of the best model decreased from 3.59%±4.27% to 3.19%±3.04%. Curves of the error versus the reflectance as depicted in Fig. 2(b) revealed that the error for the highly absorbing media decreased to about 8%. After the two-step training process, the F-ANN models had been prepared to solve the inverse problem.

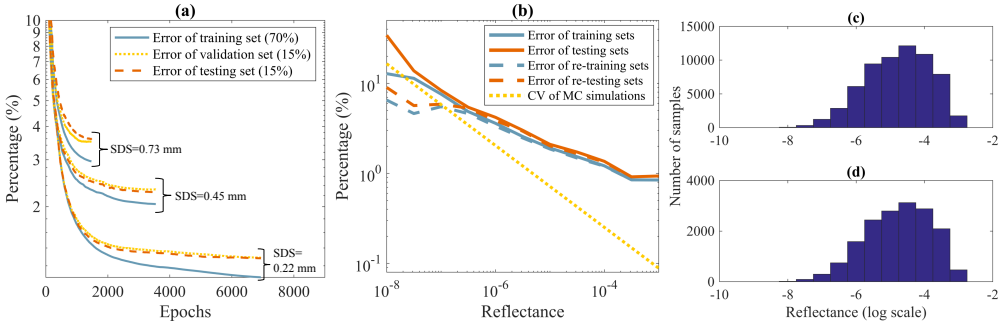

Fig. 2. (a) The error versus the number of training epochs was obtained by modelling the diffuse reflectance at each SDS with the best F-ANN model in Table 3. The training time for each epoch was around 0.15s. (b) The curves of CV versus reflectance and error versus reflectance. (c) The histogram of the reflectance collected at three SDSs in the training set. (d) The histogram of the reflectance collected at three SDSs in the testing set.

Table 3. Mean and standard deviation of the absolute relative error of the F-ANN models.

	1st training	1st training	1st training	2nd training
Neurons	SDS=0.22 mm	SDS=0.45 mm	SDS=0.73 mm	SDS=0.73 mm
[15 15]	1.57%±1.45%	2.56%±2.73%	3.97%±4.85%	3.53%±3.38%
[25 25]	1.39%±1.27%	2.31%±2.46%	3.68%±4.31%	3.21%±3.05%
[35 35]	1.35%±1.21%	**2.27%±2.40%**	3.69%±4.29%	3.21%±3.05%
[45 45]	1.35%±1.23%	2.29%±2.44%	3.65%±4.34%	**3.19%±3.04%**
[55 55]	**1.28%±1.19%**	2.27%±2.46%	3.61%±4.36%	3.19%±3.07%
[65 65]	1.38%±1.26%	2.28%±2.45%	**3.59%±4.27%**	3.24%±3.08%
[75 75]	1.38%±1.26%	2.31%±2.49%	3.70%±4.45%	3.40%±3.17%
[85 85]	1.29%±1.24%	2.36%±2.50%	3.63%±4.27%	3.31%±3.15%

Biomedical Optics EXPRESS

3.2. Validations of F-ANN models with simulated DRS data

Fifteen sets of fitting parameters were randomly sampled to generate optical coefficients over a wavelength range of 410 to 760 nm. The generated coefficients combined with fixed thicknesses of 15, 15 and 30 μm for the upper three layers were used to model diffuse reflectance spectra. 3% random Gaussian noise was added to the spectral data to simulate experimental errors. The initial guess and the iterative curve-fitting method described in Sec. 2.4 were repeated for 100 times to find an optimal set of fitting parameters. Root-mean-squared percent errors of the recovered optical coefficients, absolute relative errors of the estimated chromophore concentrations and absolute errors of the oxygen saturation for 15 sets of MC-simulated data were summarized in Table 4. Curve fitting results of MC-simulated data were depicted in Fig. 3.

The results revealed that the scattering coefficient of the stratum corneum (μ_{s1}) had the largest root-mean-squared error on average among all the optical coefficients. The reason was that the stratum corneum was a highly forward-scattering and thin layer. The partial derivative of the objective function with respect to μ_{s1} was very low. Therefore, the recovering accuracy of μ_{s1} was susceptible to the noise interference. Based on the same reason, the recovering accuracies of μ_{s2} and μ_{s3} were also limited. This issue could be improved by using oblique fibers to enhance the sensitivity to the scattering coefficient of the epithelium [32, 33]. On the contrary, μ_{a3}, μ_{a4} and μ_{s4} had great fitting accuracy since the objective function was sensitive to their variations. In addition, the means and standard deviations of the errors of the estimated chromophore information were 3.25%±2.87%, 3.59%±2.60% and 1.63%±1.40% for f_m, f_b, and S respectively. The theoretical evaluation validated that the proposed method could accurately extract the chromophore information with a high degree of accuracy.

Table 4. Errors of the recovered optical coefficients and the estimated chromophore information. The means and the standard deviations (STD) were calculated over all the samples.

Sample	μ_{s1}	μ_{s2}	μ_{a3}	μ_{s3}	μ_{a4}	μ_{s4}	f_m	f_b	S
1	11.3%	1.60%	0.71%	1.60%	0.90%	2.27%	0.72%	1.23%	0.72%
2	8.26%	5.10%	0.70%	5.10%	2.62%	1.54%	0.72%	5.31%	1.53%
3	52.1%	39.5%	10.8%	39.5%	3.03%	1.84%	6.88%	4.47%	2.91%
4	29.5%	2.16%	8.94%	2.16%	4.03%	2.29%	9.96%	7.27%	1.69%
5	13.1%	9.52%	0.37%	9.52%	2.14%	3.89%	0.38%	4.64%	2.19%
6	5.89%	10.3%	5.22%	10.3%	2.16%	3.01%	5.44%	3.69%	0.97%
7	10.4%	4.72%	5.10%	4.72%	4.40%	1.43%	5.25%	7.56%	0.16%
8	67.1%	30.7%	3.72%	30.7%	1.10%	3.12%	4.05%	0.58%	2.18%
9	28.8%	2.31%	1.07%	2.31%	0.12%	3.29%	1.12%	0.24%	0.24%
10	11.2%	5.46%	0.30%	5.46%	0.71%	0.86%	0.30%	1.02%	0.71%
11	19.9%	10.4%	1.72%	10.4%	3.27%	1.02%	1.78%	7.24%	5.37%
12	26.4%	40.3%	2.13%	40.3%	0.91%	2.98%	2.17%	1.59%	0.40%
13	34.9%	16.8%	5.33%	16.8%	0.53%	7.00%	5.44%	0.58%	0.68%
14	46.5%	3.00%	3.24%	3.00%	2.06%	3.26%	3.48%	3.53%	3.19%
15	22.8%	4.69%	1.00%	4.69%	2.43%	2.01%	1.04%	4.91%	1.51%
Mean	25.9%	12.4%	3.36%	12.4%	2.24%	2.56%	3.25%	3.59%	1.63%
STD	17.9%	13.4%	3.21%	13.4%	1.81%	1.57%	2.87%	2.60%	1.40%

Biomedical Optics EXPRESS

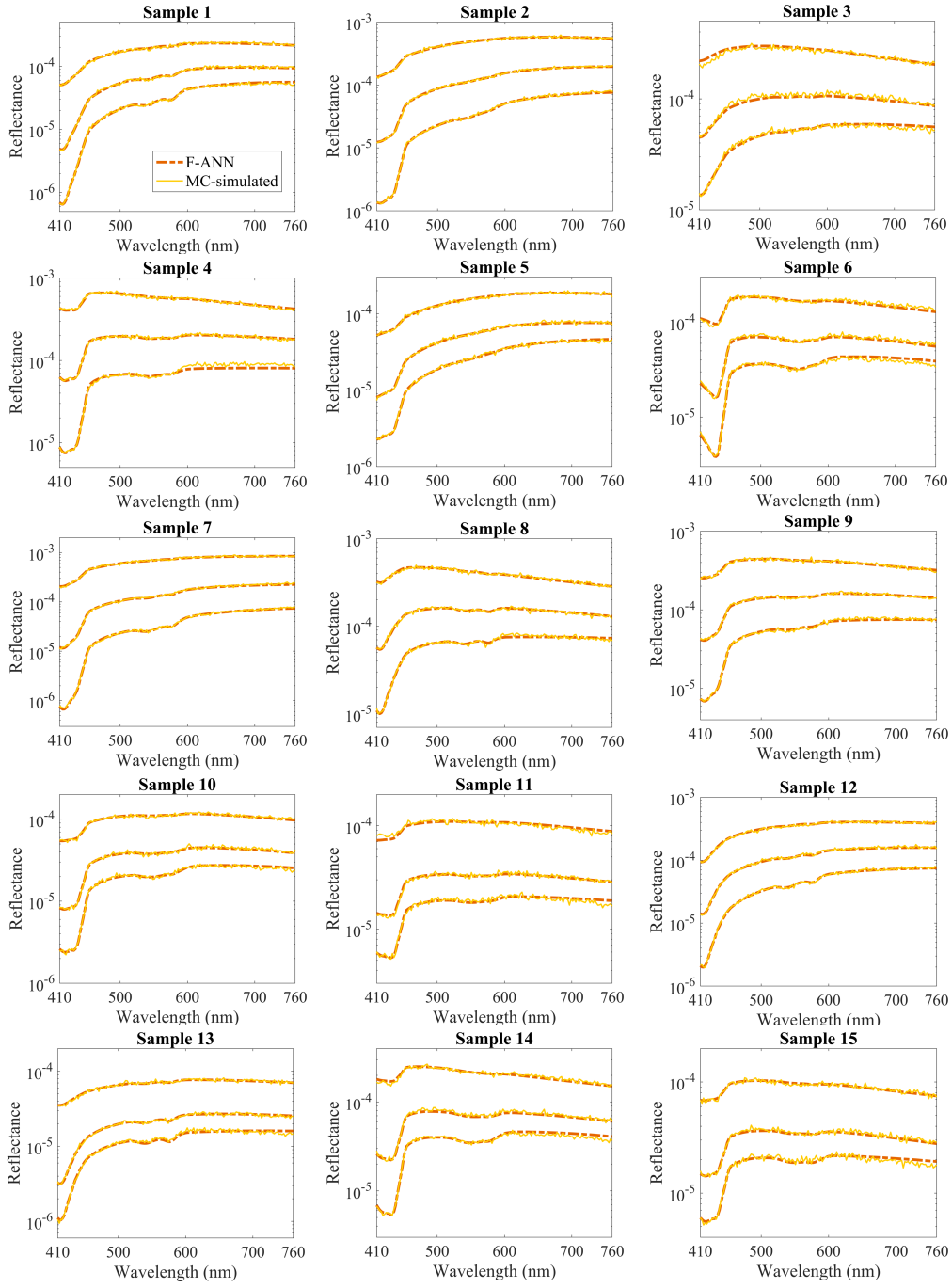

Fig. 3. Curve fitting results of 15 sets of MC-simulated data.

Biomedical Optics EXPRESS

3.3. The application of F-ANN models to extract chromophore information from *in vivo* experiments

Diffuse reflectance spectra of three different parts of the skin (i.e. face, ventral arm and dorsal arm) from three healthy human subjects were obtained by the DRS system described in Sec. 2.5. In our previous study, we found that the error of extracting optical coefficients from two-layered tissue phantoms would be reduced if the thickness information was known [34]. Therefore, HGM with sub-micrometer resolution was used to non-invasively measure the thicknesses of the stratum corneum and the other two epidermal layers (th_1, th_2, th_3). The F-ANN models were then applied to extract chromophore concentrations and oxygen saturation in the multi-layered skin tissue. After 100 times of the optimization process with different initial guesses, the optimal set of fitting parameters along with its corresponding diffuse reflectance spectra and optical coefficients was shown in Table 5 and Fig. 4. The fitting results indicated that the volume fraction of melanin (f_m) in the epidermis varied from 8.23% to 17.5% which was defined as moderately pigmented skin [31]. The average volume fraction of blood (f_b) in the dermis was around 0.2% [20] which was slightly lower than the typical value. The two dips in reflectance spectra at around 540 nm and 575 nm depicted in Fig. 4 corresponded to the high level of oxygen saturation (S) [30]. The stratum corneum had the strongest scattering property of all the layers, which was consistent with our previous research [24]. The scattering coefficients of the dermis were approximately from 150 to 60 cm^{-1} with the wavelengths ranging from 410 to 760 nm while the scattering coefficients of the lower two epidermal layers of the dorsal arm was greater than those of the face and the ventral arm. In addition, the fitted diffuse reflectance spectra showed a small mismatch from 450 nm to 700 nm in Fig. 4. Based on our previous studies, the mismatch would cause about 10% RMSE between the fitted and the measured diffuse reflectance spectra [18,33]. There were several factors that influenced the fitting performance for *in vivo* experiments: (1) optical properties of each layer in the skin model are not totally homogeneous, and (2) the tissue scattering phase function may be different from our assumption. The RMSE would be reduced if these issues were solved. To further validate the F-ANN's performance, the MC simulation was implemented to generate diffuse reflectance spectra. The optical coefficients used in the forward simulations were derived from the fitting results of the F-ANN. The root-mean-squared percent error of the MC-simulated and the measured diffuse reflectance spectra was then calculated and denoted as RMSE' in Table 5. The results showed that the F-ANN models could accurately map the fitted parameters into the corresponding spectra since the diffuse reflectance spectra obtained from the F-ANN models and the MC simulations matched well as shown in Fig. 4.

For comparison of the performance of solving the inverse problem, we implemented the identical fitting process once for each DRS measurement using MC simulations accelerated by the GPU (GPU-MC) to obtain diffuse reflectance. The fitting result of GPU-MC was also summarized in Table 5. The relative deviations between the chromophore information extracted by the two methods were about 10%, 35% and 10% for f_m, f_b, and S respectively. The RMSE revealed that the F-ANN had a better fitting performance than the GPU-MC. The primary reason was that the variation of MC simulations induced a noisy objective function, which prevented the RMSE from converging to an optimal minimum. Due to the noisy issue, finite differences of each fitting parameter should be carefully chosen to accurately calculate the gradients of the objective function. The issue can be improved by sacrificing the computation time for reducing the variation of MC simulations. In contrast, F-ANN models had a relatively smooth objective function. As a result, more than half of the tried initial guesses approached to the values with the minimal RMSE. Conclusively, the experiment showed that the F-ANN was a robust modelling method of solving the inverse problem, and the fitting speed of F-ANN models was approximately 1,000 times faster than that of GPU-MC simulations.

Biomedical Optics EXPRESS

Table 5. The fitting results of the F-ANN and the GPU-MC.

	Skin	th_1	th_2	th_3	f_m	f_b	S	RMSE	RMSE'
F-ANN	Face	10.8	28.8	27.0	8.23%	0.20%	100%	10.4%	10.6%
	Ventral arm	16.2	19.8	12.6	11.3%	0.18%	93%	8.77%	9.06%
	Dorsal arm	12.5	10.4	17.0	17.2%	0.14%	100%	13.2%	13.3%
GPU-MC	Face	10.8	28.8	27.0	7.61%	0.14%	93%	15.4%	-
	Ventral arm	16.2	19.8	12.6	12.6%	0.16%	89%	13.1%	-
	Dorsal arm	12.5	10.4	17.0	16.1%	0.27%	84%	17.0%	-

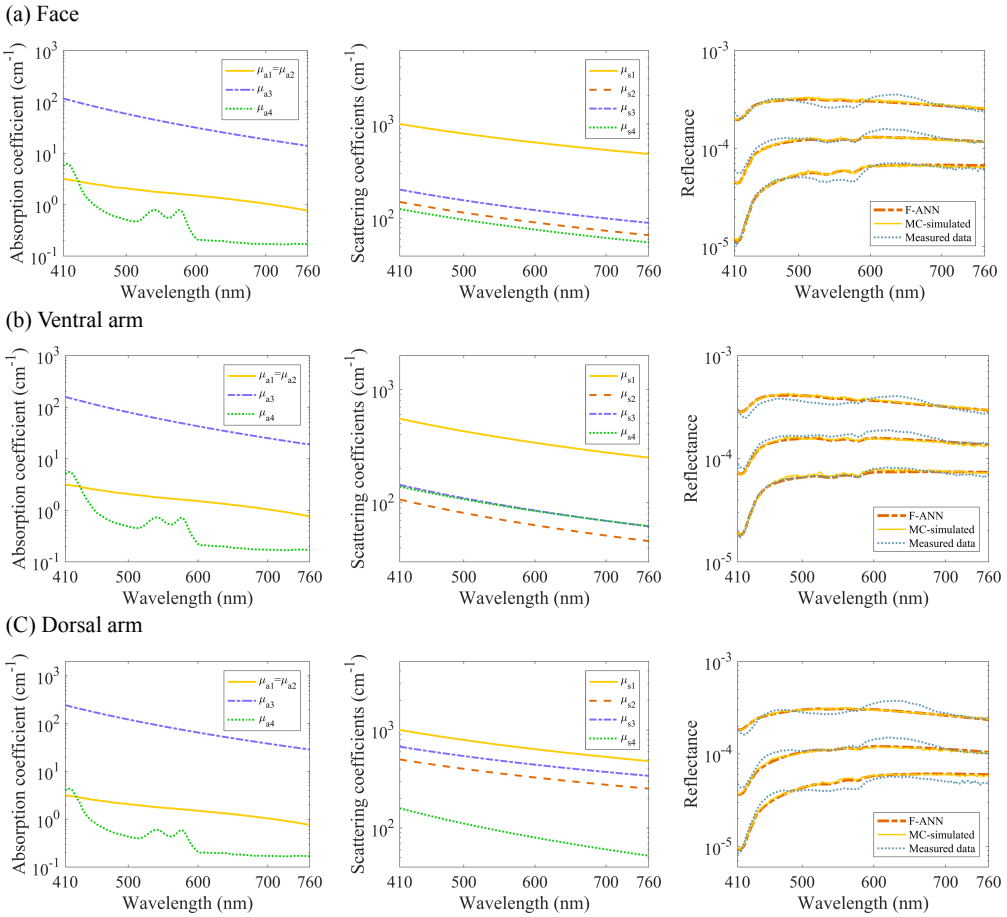

Fig. 4. (a)(b)(c) The curve fitting results of the optical coefficients and the diffuse reflectance spectra for three different parts of the skin.

4. Discussion

This study presented detailed descriptions of using F-ANN modelling method to solve the inverse problem of fitting spatially-resolved diffuse reflectance spectra. The built models could forward map a wide range of input parameters into the diffuse reflectance and inversely determine the chromophore information in the superficial multi-layered skin tissue. In addition to training three F-ANN models, one for each SDS, we tested whether a single F-ANN model could describe different SDSs. Unfortunately, the result showed that the F-ANN model failed to describe different

Biomedical Optics EXPRESS

radiative transfer functions simultaneously. It indicated different radiative transfer functions could not share the same hidden layers. As a result, F-ANN models were built separately for each SDS. Despite the minor drawback, F-ANN shows distinct features and advantages over other methods summarized in Table 6. The gold standard approach, Monte Carlo simulations, can inversely resolve optical coefficients without suffering limitations from specific geometries of the tissue, light source or detectors. However, achieving small variations of MC simulations requires huge computation cost. Even though several techniques have been proposed to address the issue, it is still time-consuming to determine optical coefficients of superficial multi-layered tissue models using spatially-resolved DRS. For example, our previous studies showed that both scalable MC and GPU-MC simulations took around one day to iteratively curve-fit a set of spectra from a single measurement [32, 33]. In contrast, the optimization process in the proposed modelling method is finished within a few minutes. Moreover, the variation of MC simulations may result in less desirable fitting results due to the noisy objective function.

Table 6. Comparisons of different modelling methods.

Method	Accuracy	Time cost	Limitation	Database
MC	High	High	No	No
SE/EMs	Medium	Medium	High	Small
LUT	High	Medium	Low	Large
I-ANN	Low	Low	Medium	Medium
F-ANN	High	Medium	Low	Medium

Loop-up-table is a numerical method of estimating new values of diffuse reflectance by interpolating a discrete set of known parameters. The accuracy could be very high when the database is sufficiently large and the variation of MC simulations is controlled [35, 36]. The main disadvantage of the LUT method is that evenly spaced increments for each optical parameter of interest are required for the interpolation, which implies that the database tends to be very large. As a result, only three or four-dimensional LUT has been developed to extract physiological parameters and optical properties of two-layered tissue [12, 13]. For example, Sharma *et al.* used 20 evenly spaced increments each for four free parameters to generate a database with 160,000 samples [13]. By contrast, F-ANN has an ability to efficiently solve the nonlinear relationship between input parameters and the target reflectance. The input parameters can be randomly sampled, and a smaller database is sufficient to generate a robust F-ANN model.

I-ANN is a popular method that can directly determine optical coefficients without using any iterative optimization process. However, several studies showed that I-ANN models had large prediction errors [37–42]. To improve the accuracy, checking the uniqueness of mapping reflectance sets into corresponding optical parameters is needed [43]. Due to the uniqueness issue, the recovery ability of I-ANN models is limited to one or two-layered tissue. By contrast, the structure of the multi-layered F-ANN model was closer to real skin structures. It would provide more realistic information about the skin than one or two-layered tissue models [11]. Moreover, the I-ANN method lacks the advantage of using the prior knowledge of wavelength dependences of optical coefficients. A post-fitting process was needed to apply wavelength-dependent expressions to the predicted optical coefficients obtained from I-ANN models [14]. Although F-ANN requires more computation than I-ANN, it can avoid the uniqueness issue and improve both the accuracy and robustness of extracting optical properties using broadband spectra.

Compared to LUT, I-ANN and F-ANN modelling methods, semi-empirical/empirical methods require smaller databases to build forward models for diffuse reflectance emitted from the tissue. However, the disadvantage of SE/EMs is that they can only be applied to specific conditions. For example, several models assumed tissue to be a one-layered homogeneous turbid medium [44, 45]; two-layered tissue models assumed either the upper or bottom layer to be strongly forward

Biomedical Optics EXPRESS

scattering [9, 10, 46, 47]; multi-layered tissue models assumed that scattering properties are equal for all layers [11]. The numerical F-ANN model, by contrast, is versatile and not subject to the above limitations.

Due to the robustness and efficiency, F-ANN is a promising tool to replace time-consuming MC simulations for many applications. The proposed method can be used to extract optical properties for different kinds of biological tissues such as mucosa in the digestion track, the breast, brain, skin, subcutaneous fat and muscle tissues. Combined with wavelength-dependent expressions, the modelling technique is capable of solving chromophore information in multi-layered tissues. It is also well suited to be applied to the spatial-frequency-domain DRS [15, 16], frequency-domain DRS [48], and image-based DRS such as modulated imaging [49] and hyperspectral imaging [50].

5. Conclusion

Spatially-resolved diffuse reflectance spectroscopy has been employed to analyze optical properties of biological tissue. This work presented a modelling method of extracting scattering coefficients, chromophore concentrations and oxygen saturation in multi-layered skin tissue based on F-ANN models for *in vivo* DRS measurements. Through the two-step training process, the models accurately mapped nine parameters including three thicknesses and six optical coefficients into diffuse reflectance spectra. The results showed that absolute relative errors of models were 1.28%±1.19%, 2.27%±2.40% and 3.19%±3.04% for the three optical fibers separated from the source fiber by distances of 0.22 mm, 0.45 mm and 0.73 mm, respectively. The built models were then used to extract optical properties of MC-simulated spectra for theoretical validations. It was shown that the F-ANN models could accurately estimate chromophore information while noise interference would affect the accuracy of recovering scattering properties of epidermal layers especially for the stratum corneum. To further demonstrate the model's applicability, diffuse reflectance spectra of three different parts of the skin (i.e. face, ventral arm and dorsal arm) were measured *in vivo* by a custom-built DRS system. The thicknesses of three epidermal layers were pre-determined by *in vivo* harmonic generation microscopic imaging. The chromophore information of the skin tissue was then obtained by iteratively curve-fitting the F-ANN models and estimating optical coefficients with known wavelength dependences. The experimental results demonstrated that the F-ANN models can significantly reduce the computation time with a better fitting performance compared to GPU-MC simulations. Due to the robustness and efficiency, F-ANN is a promising tool for many applications. In the future, we would implement F-ANN models for the diagnosis of diseases and characterization of physiological conditions of tissues.

Funding

The Ministry of Science and Technology, Taiwan (MOST) (105-2221-E-002-068-MY3).

Disclosures

The authors declare that there are no conflicts of interest related to this article.